Fractional anisotropy as a tracer of cosmic voids

Sebastian Bustamante $\star^{1}$, Jaime E. Forero-Romero^{2}

^{1}*Instituto de Física - FCEN, Universidad de Antioquia, Calle 67 No. 53-108, Medellín, Colombia*
^{2}*Departamento de Física, Universidad de los Andes, Cra. 1 No. 18A-10, Edificio Ip, Bogotá, Colombia*

ABSTRACT
Finding and characterizing underdense regions (voids) in the large scale structure of the Universe is an important task in cosmological studies. In this paper we present a novel approach to find voids in cosmological simulations. Our approach is based on algorithms that use the tidal and the velocity shear tensors to locally define the cosmic web. Voids are identified using the fractional anisotropy (FA) computed from the eigenvalues of each web scheme. We define the void boundaries using a watershed transform based on the local minima of the FA and its boundaries as the regions where the FA is maximized This void identification technique does not have any free parameters and does not make any assumption on the shape or structure of the voids. We test the method on the Bolshoi simulation and report on the density and velo ity profiles for the voids found using this new scheme.

Key words: Cosmology: theory - large-scale structure of Universe - Methods: data analysis - numerical - N-body simulations

1 INTRODUCTION

Since voids were found in the first compiled galaxy surveys they have been identified as one of the most striking features of the Cosmic Web (Chincarini & Rood 1975; Gregory & Thompson 1978; Einasto et al. 1980a,b; Kirshner et al. 1981, 1987; Bond et al. 1996). However, due to the large volume extension of void regions ($\sim 5-10\,\mathrm{Mpc}h^{-1}$), statistically meaningful catalogues of voids (Pan et al. 2012; Sutter et al. 2012; Nadathur & Hotchkiss 2014) have only become available through modern galaxy surveys like the two-degree field Galaxy Redshift Survey (Colless et al. 2001, 2003) and the Sloan Digital Sky Survey (York et al. 2000; Abazajian et al. 2003). This advancement generated a great interest to study voids observationally during the last decade (Hoyle & Vogeley 2004; Croton & et al. 2004; Rojas et al. 2005; Ceccarelli et al. 2006; Patiri et al. 2006; Tikhonov 2006; Patiri et al. 2006; Tikhonov 2007; von Benda-Beckmann & Müller 2008; Foster & Nelson 2009; Ceccarelli et al. 2013; Sutter et al. 2014).

On the theoretical side, early descriptions of the evolution of the large-scale Universe, based on gravitational instabilities in primordial stages and leaded by the seminal work of Zel'dovich (1970), are consistent with the Cosmic Web picture, where planar pancake-like regions of matter enclose enormous underdense voids and are bordered, in turn, by thin filaments and high-density clumpy knots (Bond

et al. 1996). First theoretical models for describing formation, dynamics and properties of voids (Hoffman & Shaham 1982; Icke 1984; Bertschinger 1985; Blumenthal et al. 1992) were dramatically complemented and extended by first numerical studies based on simulations (Martel & Wasserman 1990; Regos & Geller 1991; van de Weygaert & van Kampen 1993; Dubinski et al. 1993). This tendency of using numerical data from N-body simulations, fuelled by last generation computing systems and ever more efficient numerical algorithms, has become increasingly common in the last years as a powerful analysis toolkit of cosmic voids (for an extensive compilation of previous numerical works, see Colberg et al. (2008)).

At present, studying voids may be considered as a threefold enterprise (Platen et al. 2007): first, they are a key ingredient of the Cosmic Web as they dominate almost the entire volume distribution at large-scales and additionally, they compensate overdense structures in the total budget of matter. This implies that a full understanding of their evolution and properties is essential for fathoming the high complexity of the Cosmic Web. Second, they provide a valuable resource for inferring and probing cosmological parameters as their structure and dynamics are highly determined by these values. Third, they constitute an unique and still largely pristine environment in which can be tested galaxy evolution.

Although a visual recognition of voids in galaxy surveys and simulations is possible in most cases, a formal systematic identification is necessary for statistically meaningful

$\star$ sebastian.bustamante@udea.edu.co

studies. However, a basic yet essential issue remains regarding the definition itself of what a void is. There is not a general consensus about an unambiguous definition of cosmic voids and therefore, there can be found many different void finding techniques throughout the literature (for a detailed comparison of different schemes, see the Void Finder Comparison Project Colberg et al. (2008)). In spite of the diversity of existing schemes, they can be roughly classified into two main types: first, geometric schemes based on point spatial or redshift distribution of galaxies in surveys or catalogues of dark matter halos in simulations (Kauffmann & Fairall 1991; Müller et al. 2000; Gottlöber et al. 2003; Hoyle & Vogeley 2004; Brunino et al. 2007; Foster & Nelson 2009; Micheletti & et al. 2014; Sutter et al. 2014), and second, schemes based on the smooth and continuous matter density field either from simulations or from reconstruction procedures on surveys (Plionis & Basilakos 2002; Colberg et al. 2005; Shandarin et al. 2006; Platen et al. 2007; Neyrinck 2008; Neyrinck et al. 2013; Ricciardelli et al. 2013).

Here we introduce a new tracer of the structure of cosmic voids built from two tensorial web schemes, i.e. the Tweb, based on the Hessian of the gravitational potential or tidal tensor (Hahn et al. 2007; Forero-Romero et al. 2009), and the Vweb, based on the velocity shear tensor (Hoffman et al. 2012). These web schemes classify the Cosmic Web into four different types of environment depending on the counting of the number of eigenvalues below an user-defined threshold (λ_{th}), namely voids (3 eigenvalues below λ_{th}), sheets (2), filaments (1) and knots or clusters (0). The tidal and the shear tensors have proven to be more fundamental than the density field as they also trace the collapsing or expanding nature of the matter field, which ultimately is what defines the underlying dynamics of the Cosmic Web. Furthermore, the density field is degenerated regarding the defined types of environment (Hahn et al. 2007), which implies that is not possible to assign a priori a range of density values to each of them. This yields that the usually adopted definition of voids as simply underdense regions in the large-scale matter distribution, is not precise enough as it excludes a proper description of the internal structure of voids.

Following the recent trend of using digital image-processing techniques developed in other disciplines (e.g. medical sciences and computer imaging) for analysing the structure of the Cosmic Web, we propose here, much in the same way as Libeskind et al. (2013), the fractional anisotropy (FA) as a tracer of the internal structure and the outline of cosmic voids. The FA was initially introduced by Basser (1995) for quantifying the anisotropy degree of the diffusivity of water molecules through cerebral tissue in nuclear magnetic resonance imaging. In this context we use the same quantity for determining the anisotropy degree of the local environment from either the orbital dynamics as set by the eigenvalues of the tidal tensor (Tweb), or the dynamics of the velocity field as set by the eigenvalues of the shear tensor (Vweb). In both cases, the FA is not determined directly from the density field, it hence is suitable for describing both, the structure of high non-linear regions (e.g. filaments, knots and very dense walls) as well as the fainter substructure exhibited by quasi-linear regions like voids.

Once established the FA as the tracer field of cosmic voids, we proceed to identify individual voids as basins of local minima. For this purpose we implement a technique developed by Beucher & Lantuejoul (1979) and Beucher & Meyer (1993) and widely used in the field of image analysis and mathematical morphology, i.e. the *watershed transform algorithm*. This technique has been already implemented on void finding schemes by Platen et al. (2007) and Neyrinck (2008) with very interesting results, where individual voids are identified as catching basins of local minima of the density field. The appeal of this algorithm consists in that is parameter-free and does not require any assumption on the shape and morphology of voids. Although we use a *cloud-in-cell* (CIC) algorithm on a Cartesian mesh for estimating the density and tensor fields, instead of the more sophisticated *Delaunay tessellation for field estimator* (DTFE) technique (Schaap & van de Weygaert 2000), our implementation of the watershed transform should not be significantly affected as we are interested in low density regions where the CIC gives similar estimations.

This paper is organized as follows. In section 2 we describe the used simulation for testing our void finding algorithm, i.e. the Bolshoi simulation. A detailed description of these methods is presented in section 3. In section 4 we describe how the FA can be used for tracing the structure of voids. Once obtained meaningful catalogues of voids for each scheme, we proceed to compare some typical and general interest properties of voids such as volume functions, distributions of size and density and velocity profiles. This is done in section 5. Finally in section 6 we analyse and evaluate our findings.

2   THE SIMULATION

We use here an unconstrained cosmological simulation (the Bolshoi simulation) to identify the possible large scale environment and the distribution of cosmic voids at $z = 0$. The Bolshoi simulation follows the non-linear evolution of a dark matter density field on a cubic volume of size $250h^{-1}\mathrm{Mpc}$ sampled with 2048^3 particles. The cosmological parameters in the simulation are $\Omega_m = 0.27$, $\Omega_\Lambda = 0.73$, $h = 0.70$, $n = 0.95$ and $\sigma_8 = 0.82$ for the matter density, cosmological constant, dimensionless Hubble parameter, spectral index of primordial density perturbations and normalization for the power spectrum respectively, consistent with the seventh year of data of the Wilkinson Microwave Anisotropy Probe (WMAP) (Jarosik et al. 2011). For more detailed technical information about the simulation, see Klypin et al. (2011).

For estimating the density and velocity fields we use a *cloud-in-cell* (CIC) algorithm onto a grid of 256^3 cells, corresponding to a resolution of $0.98h^{-1}\mathrm{Mpc}$ per cell side. Then, through finite-differences and FFT methods the tidal and shear tensors are computed. Finally, the eigenvalues and eigenvectors of the tensor are obtained for each cell of the grid. Neglecting substructures presented below Megaparsec scales and taking into account our focus in voids, which are a prominent characteristic of the Megaparsec Universe, we apply a Gaussian softening of one cell to all fields.

3 ALGORITHMS TO QUANTIFY THE COSMIC WEB

3.1 The tidal web (Tweb)

This scheme was initially proposed by Hahn et al. (2007) as a novel alternative for classifying the Cosmic Web based on the tidal tensor, that is somehow more fundamental than the density field as it also allows to quantify the orbital dynamics of the matter field. This approach consists of a second-order expansion of the equations of motion around local minima of the gravitational potential and then extended to any position. The second-order term corresponds to the tidal tensor, which is defined as the Hessian matrix of the normalized gravitational potential

$$T_{\alpha\beta} = \frac{\partial^2 \phi}{\partial x_\alpha \partial x_\beta} \tag{1}$$

where the physical gravitational potential has been rescaled by a factor $4\pi G\bar{\rho}$ in such a way that ϕ satisfies the following equation

$$\nabla^2 \phi = \delta, \tag{2}$$

with $\bar{\rho}$ the average density in the Universe, G the gravitational constant and δ the dimensionless matter overdensity.

Since the tidal tensor can be represented in any cell by a real and symmetric 3×3 matrix, it is ensured the possibility to diagonalize it and obtain three real eigenvalues $\lambda_1 \geqslant \lambda_2 \geqslant \lambda_3$. This set of eigenvalues can be used as indicators of the local orbital stability in each proper direction, which in turn can be translated into a classification scheme of the Cosmic Web. A counting of the number of positive (stable) or negative (unstable) eigenvalues allows to catalogue a single cell into one of the next four types of environment: voids (3 negatives eigenvalues), sheets (2), filaments (1) and knots (0). A significant improvement to this scheme was introduced by Forero-Romero et al. (2009) by means of a relaxation of the stability criterion. The relative strength of each eigenvalue is no longer defined by the sign, but instead by a threshold value λ_{th} that can be tuned in such a way that the visual impression of the web-like matter distribution is reproduced.

3.2 The velocity web (Vweb)

We also use a kinematical scheme to define the Cosmic Web environment in the simulation. The scheme has been thoroughly described in Hoffman et al. (2012) and applied to study the shape and spin alignment in the Bolshoi simulation in Libeskind et al. (2013). We refer the reader to these papers to find a detailed description of the algorithm, its limitations and capabilities. The Vweb scheme for environment finding is based on the local velocity shear tensor calculated from the smoothed dark matter velocity field in the simulation. The central quantity is given by the following dimensionless expression

$$\Sigma_{\alpha\beta} = -\frac{1}{2H_0}\left(\frac{\partial v_\alpha}{\partial x_\beta} + \frac{\partial v_\beta}{\partial x_\alpha}\right) \tag{3}$$

where v_α and x_α represent the α component of the comoving velocity and position, respectively. Like the tidal tensor, $\Sigma_{\alpha\beta}$ can be represented by a 3×3 symmetric matrix with real values, hence diagonalizing it is obtained three real eigenvalues $\lambda_1 \geqslant \lambda_2 \geqslant \lambda_3$ whose sum (the trace of $\Sigma_{\alpha\beta}$) is proportional to the divergence of the local velocity field smoothed on the physical scale $\mathcal{R}$.

In the same way, the relative strength of the three eigenvalues with respect to a threshold value λ_{th} allows for the local classification of the matter distribution into the previous four web types. For the threshold choosing in both schemes, the Tweb and the Vweb, it is usual to fine-tuning the value in such a way that the visual appearance of the Cosmic Web as seen in simulations and galaxy surveys is reproduced. However, we do not take this approach here, instead we propose a novel approach for the threshold choosing based on the maximization of the fractional anisotropy field occurring in filaments and very dense walls.

4 FINDING VOIDS

4.1 The fractional anisotropy

The fractional anisotropy (FA), as developed by Basser (1995), was conceived to quantify the anisotropy degree of a diffusion process, e.g. the diffusivity of water molecules through cerebral issue in nuclear magnetic resonance imaging. Here we propose the FA, much in the same way as Libeskind et al. (2013), as a tracer of cosmic voids.

$$FA = \frac{1}{\sqrt{3}}\sqrt{\frac{(\lambda_1 - \lambda_3)^2 + (\lambda_2 - \lambda_3)^2 + (\lambda_1 - \lambda_2)^2}{\lambda_1^2 + \lambda_2^2 + \lambda_3^2}} \tag{4}$$

where the eigenvalues are taken from either the Tweb or the Vweb (FA-Tweb and FA-Vweb respectively). Such as it is defined, $FA = 0$ corresponds with an isotropic dynamic and $FA = 1$ with a highly anisotropic distribution.

In left panels of Fig. 1 we calculate the FA for both web schemes over a slide of the simulation. Some important points can be concluded from this figure:

• Voids display a highly isotropic expanding dynamic at their centres, becoming gradually more anisotropic at outer regions.

• Knots feature with very isotropic collapses. For the Tweb, the FA exhibits very narrow distribution around knots. For the Vweb, these distributions are more spread out, thereby indicating strong differences between the density and the velocity fields in highly non-linear regions.

• The filamentary structure of the Cosmic Web is well traced by high FA values (black regions), thus indicating very anisotropic dynamics for sheets and filaments.

• The FA, unlike the density field, displays a non-monotonic behaviour, where low values are characteristic of central regions of voids, reaching high values in sheets and filaments and becoming low again in knots.

4.2 Voids using web schemes

For both web schemes, voids are regions where $\lambda_3 \leqslant \lambda_2 \leqslant \lambda_1 \leqslant \lambda_{th}$. This implies that the outlines of voids are

completely fixed by the relative strength of the λ_1 eigenvalue with respect to the threshold value. Therefore, as we increase/decrease the threshold value λ_{th}, voids expand/diminish progressively through contours of λ_1. In Fig. 2 we calculate the distribution of the FA as well as of the density field with respect to λ_1 over all cells of the grid.

From Fig. 2 we conclude that the FA is a good tracer of voids as is almost perfectly correlated with low values of λ_1. Then, it reaches a maximum value, namely sheets and filaments, for finally reaching knots, which feature low FA values. This behaviour can be thought as a sort of one-dimensional tomography of the Cosmic Web. This characteristic allows us to propose an optimal threshold value for both web schemes where the FA is maximized. Specifically we propose a value of $FA = 0.95$, corresponding with a threshold $\lambda_{opt}^T = 0.265$ for the Tweb and $\lambda_{opt}^V = 0.175$ for the Vweb. For a threshold above these values, voids would span over very anisotropic regions, which must correspond to sheets and filaments. A threshold below would imply very low volume filling fractions of voids and dominant sheets. Finally, the density field do not correlate well with λ_1 (as calculated for both web schemes), and due to its monotonic increase, an estimate of an optimal threshold is not as clear as for the FA.

Once set the optimal thresholds for the web schemes, we proceed in Fig. 3 to sample the FA and the prolateness for a random sample of cells previously classified into one of the four environments. The prolateness is introduced here for differentiating sheets and filaments featuring high FA values. In order to illustrate the underlying local dynamics sampled by the cells, we also sketch different spheroidal geometries according to the relative strength of each eigenvalue, and then, we associate them to different ranges of the FA and the prolateness. From this, we conclude sheets display very anisotropic distributions, namely above $FA = 0.95$. They are also biased towards oblate geometries, however there are some elongated sheets as well. Filaments are not as anisotropic as sheets, ranging from middle up to high FA values. They exhibit prolate geometries, but a considerable fraction of them are biased towards slightly more oblate values. Voids and knots are the only environments featuring with low FA values, thus indicating very isotropic expanding/collapsing dynamics at their centres. However, voids span over a very wide range of FA and geometries, whereas knots only span over low to middle FA values and display a biased oblate geometry.

4.3   Identifying void regions through web schemes

5   PROPERTIES OF VOIDS

Once defined our method to classify bulk voids based upon web classification schemes of the cosmic web, we proceed to analyse some physical properties in order to compare their consistency with the geometry of voids as quantified by our method and by density-based schemes. Next, through the reduced inertia tensor we quantify the shape distribution of voids. Finally, we compute numerical radial profiles of density and peculiar velocity of bulk voids.

5.1   Statistics of halos in voids

One of the main challenges in observational void finding is the discrete nature of galaxy surveys

we calculate contours of discrete fields like the median mass and the local number of local dark matter halos and

, like the inertia values, the density and peculiar velocities profiles as calculated over the grid and profiles of number of halos.

5.2   Density profile of voids

Describing the density profiles of voids is quite important in order to compare and match simulation with observational surveys, allowing possible constrains for different cosmology models [**Hamaous, et.al 2014**]. Here, and taking into account the previous results, we rather use an ellipsoidal approximation to describe and fit the shape of bulk voids, so we use the next ellipsoidal radial coordinate to describe density profiles.

$$r^2 = \frac{x^2}{\tau_1^2} + \frac{y^2}{\tau_2^2} + \frac{z^2}{\tau_3^2}, \quad 0 \leqslant r \leqslant 1 \tag{5}$$

where we take the principal moments of inertia $\{\tau_i\}$ as the lengths of the principal axes of the ellipsoid and each one of the cartesian coordinates as measured in the rotated frame of each void.

We use the same analytic density profile that [**Hamaous, et.al 2014**] to fit the numerical density profiles of our voids.

$$\delta_v(r) = \delta_c \frac{1 - (r/r_s)^\alpha}{1 + (r/r_v)^\beta} \tag{6}$$

$$\mathcal{C} = \frac{M_v}{\overline{M}} = \frac{3}{2R^3} \int_0^R [\delta(r) + 1] r^2 dr$$

$$\mathcal{C} < 1$$

$$\mathcal{C} > 1$$

6   CONCLUSIONS

ACKNOWLEDGMENTS

REFERENCES

Abazajian K., et al. (the SDSS Collaboration) 2003, AJ, 126, 2081

Basser P., 1995, NMR in Biomedical Imaging, 8, 333

Bertschinger E., 1985, ApJS, 58, 1

Beucher S., Lantuejoul C., 1979, in Proceedings International Workshop on Image Processing, CCETT/IRISA, Rennes, France

Beucher S., Meyer F., 1993, Mathematical Morphology in Image Processing. Marcel Deker, New York

Blumenthal G. R., da Costa L. N., Goldwirth D. S., Lecar M., Piran T., 1992, ApJ, 388, 234

Bond J. R., Kofman L., Pogosyan D., 1996, Nature, 380, 603

Brunino R., Trujillo I., Pearce F. R., Thomas P. A., 2007, MNRAS, 375, 184

Ceccarelli L., Padilla N. D., Valotto C., Lambas D. G., 2006, MNRAS, 373, 1440

Ceccarelli L., Paz D., Lares M., Padilla N., Lambas D. G., 2013, MNRAS, 434, 1435

Chincarini G., Rood H. J., 1975, Nature, 257, 294

Colberg J. M., Pearce F., et al. 2008, MNRAS, 387, 933

Colberg J. M., Sheth R. K., Diaferio A., Gao L., Yoshida N., 2005, MNRAS, 360, 216

Colless M., et al. (the 2dFGRS Team), 2001, MNRAS, 328, 1039

Colless M., et al. (the 2dFGRS Team), 2003, VizieR Online Data Catalog, 7226

Croton D. J., et al. 2004, MNRAS, 352, 828

Dubinski J., da Costa L. N., Goldwirth D. S., Lecar M., Piran T., 1993, ApJ, 410, 458

Einasto J., Joeveer M., Saar E., 1980a, MNRAS, 193, 353

Einasto J., Joeveer M., Saar E., 1980b, Nature, 283, 47

Forero-Romero J. E., Hoffman Y., Gottlöber S., Klypin A., Yepes G., 2009, MNRAS, 396, 1815

Foster C., Nelson L. A., 2009, ApJ, 699, 1252

Gottlöber S., Łokas E. L., Klypin A., Hoffman Y., 2003, MNRAS, 344, 715

Gregory S. A., Thompson L. A., 1978, ApJ, 222, 784

Hahn O., Porciani C., Carollo C. M., Dekel A., 2007, MNRAS, 375, 489

Hoffman Y., Metuki O., Yepes G., Gottlöber S., Forero-Romero J. E., Libeskind N. I., Knebe A., 2012, MNRAS, 425, 2049

Hoffman Y., Shaham J., 1982, ApJL, 262, L23

Hoyle F., Vogeley M. S., 2004, ApJ, 607, 751

Icke V., 1984, MNRAS, 206, 1P

Jarosik N., Bennett C. L., et al. 2011, ApJS, 192, 14

Kauffmann G., Fairall A. P., 1991, MNRAS, 248, 313

Kirshner R. P., Oemler Jr. A., Schechter P. L., Shectman S. A., 1981, ApJL, 248, L57

Kirshner R. P., Oemler Jr. A., Schechter P. L., Shectman S. A., 1987, ApJ, 314, 493

Klypin A., Gottlöber S., Kravtsov A. V., Khokhlov A. M., 1999, ApJ, 516, 530

Klypin A. A., Trujillo-Gomez S., Primack J., 2011, ApJ, 740, 102

Libeskind N. I., Hoffman Y., Forero-Romero J., Gottlöber S., Knebe A., Steinmetz M., Klypin A., 2013, MNRAS, 428, 2489

Martel H., Wasserman I., 1990, ApJ, 348, 1

Micheletti D., et al. 2014, ArXiv e-prints

Müller V., Arbabi-Bidgoli S., Einasto J., Tucker D., 2000, MNRAS, 318, 280

Nadathur S., Hotchkiss S., 2014, MNRAS, 440, 1248

Neyrinck M. C., 2008, MNRAS, 386, 2101

Neyrinck M. C., Falck B. L., Szalay A. S., 2013, ArXiv e-prints

Pan D. C., Vogeley M. S., Hoyle F., Choi Y.-Y., Park C., 2012, MNRAS, 421, 926

Patiri S. G., Betancort-Rijo J., Prada F., 2006, MNRAS, 368, 1132

Patiri S. G., Prada F., Holtzman J., Klypin A., Betancort-Rijo J., 2006, MNRAS, 372, 1710

Platen E., van de Weygaert R., Jones B. J. T., 2007, MNRAS, 380, 551

Plionis M., Basilakos S., 2002, MNRAS, 330, 399

Regos E., Geller M. J., 1991, ApJ, 377, 14

Ricciardelli E., Quilis V., Planelles S., 2013, MNRAS, 434, 1192

Riebe K., Partl A. M., Enke H., Forero-Romero J., Gottloeber S., Klypin A., Lemson G., Prada F., Primack J. R., Steinmetz M., Turchaninov V., 2011, ArXiv e-prints

Rojas R. R., Vogeley M. S., Hoyle F., Brinkmann J., 2005, ApJ, 624, 571

Schaap W. E., van de Weygaert R., 2000, A&A, 363, L29

Shandarin S., Feldman H. A., Heitmann K., Habib S., 2006, MNRAS, 367, 1629

Sutter P. M., Lavaux G., Hamaus N., Pisani A., Wandelt B. D., Warren M. S., Villaescusa-Navarro F., Zivick P., Mao Q., Thompson B. B., 2014, ArXiv e-prints

Sutter P. M., Lavaux G., Wandelt B. D., Weinberg D. H., 2012, ApJ, 761, 44

Sutter P. M., Lavaux G., Wandelt B. D., Weinberg D. H., Warren M. S., 2014, MNRAS, 438, 3177

Tikhonov A. V., 2006, Astronomy Letters, 32, 727

Tikhonov A. V., 2007, Astronomy Letters, 33, 499

van de Weygaert R., van Kampen E., 1993, MNRAS, 263, 481

von Benda-Beckmann A. M., Müller V., 2008, MNRAS, 384, 1189

York D. G., et al. (the SDSS Collaboration), 2000, AJ, 120, 1579
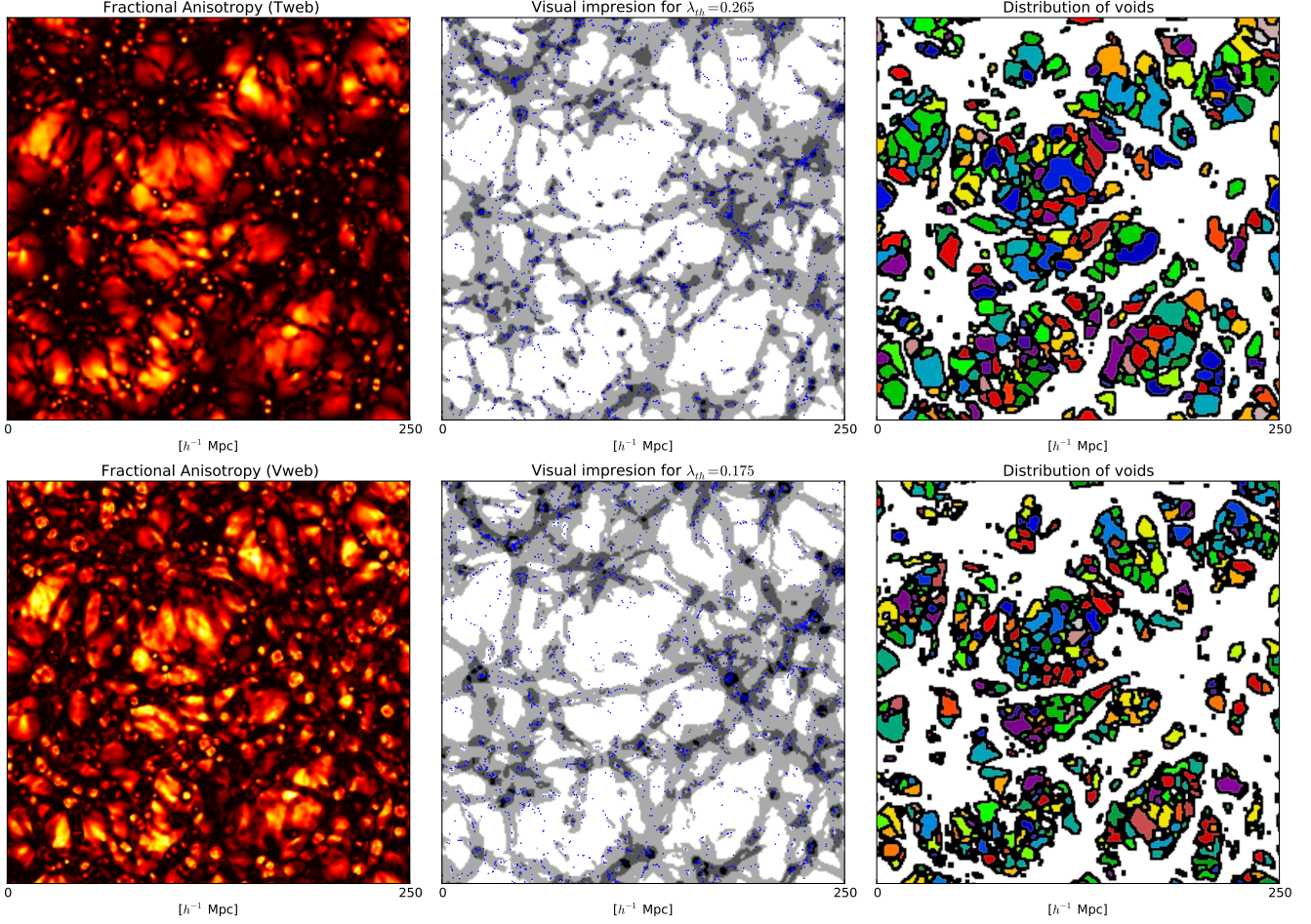
Zel'dovich Y. B., 1970, A&A, 5, 84

Figure 1. Left panels show the visual impression of the FA field over a slide of the simulation for each web scheme (T-web, upper panels. V-web, middle panels). Black regions correspond with high values, i.e. FA≈ 1, while white and light yellow regions to FA≈ 0. It is worth noting the degeneration of low values of FA for knots and central regions of voids, thus indicating a high isotropy for both processes. In the same way, high values of FA are consistent with the anisotropic geometry exhibited by filaments and very flat sheets. Middle panels sketch the components of the Cosmic Web using the optimal threshold values. Voids corresponds with white, sheets to gray, filaments to dark gray and knots with black regions. Finally right panels sketch the distribution of the catalogued voids by our method.
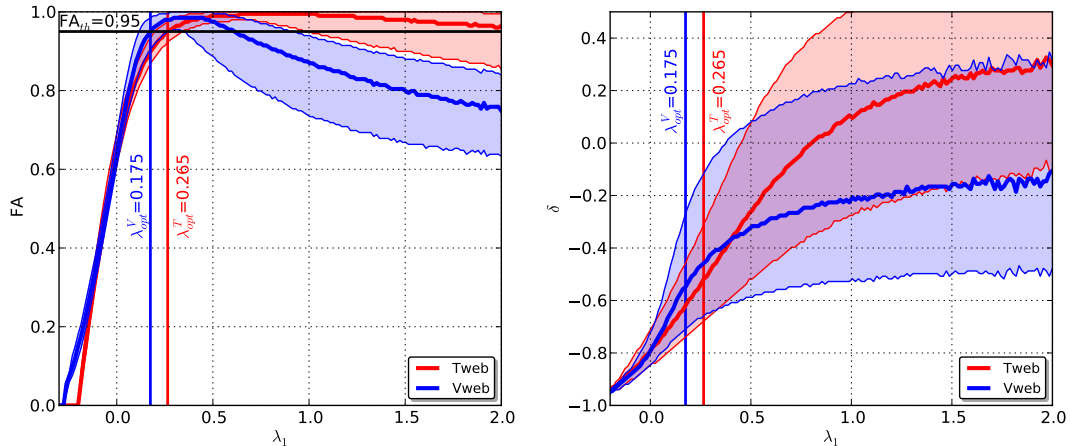

Figure 2. Distributions of the FA (left panel) and the density field (right panel) with respect to the eigenvalue λ_1 for each web scheme (Tweb, red lines. Vweb, blue lines) as calculated over all cells of the grid. Thick central lines correspond with the median and filled regions with the 50% of the distribution.
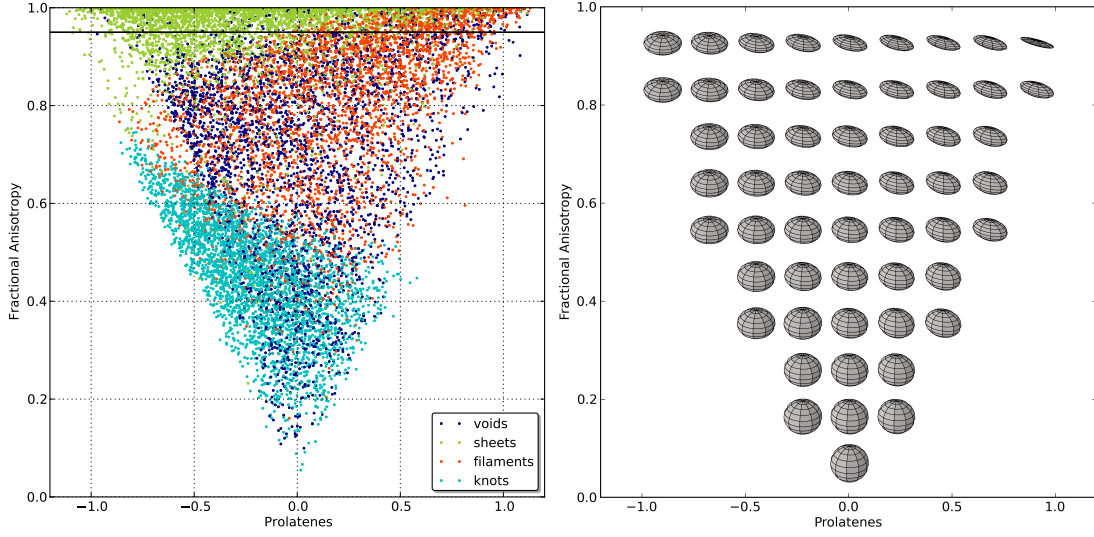
Figure 3. Fractional anisotropy and prolateness for a random sample of cells (left panel) and for different spherical geometries (right panel). For the cells, each environment is coded with a different colour, i.e. voids corresponds with dark blue points, sheets with green, filaments with orange and knots with cyan. The axis of the spheroids are computed from the relative strengths of the eigenvalues, so their shape sketch the relative expanding/collapsing dynamics into each direction.
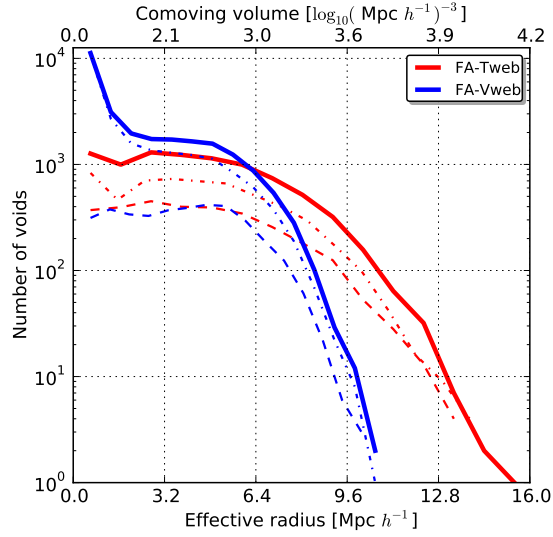

Figure 4. Volume functions of voids for both built catalogues. Watershed-Tweb (red curves), Watershed-Vweb (blue curves). Continuous lines corresponds with the total number of voids, dot-dashed with sub-compensated voids and dashed lines with over-compensated voids.
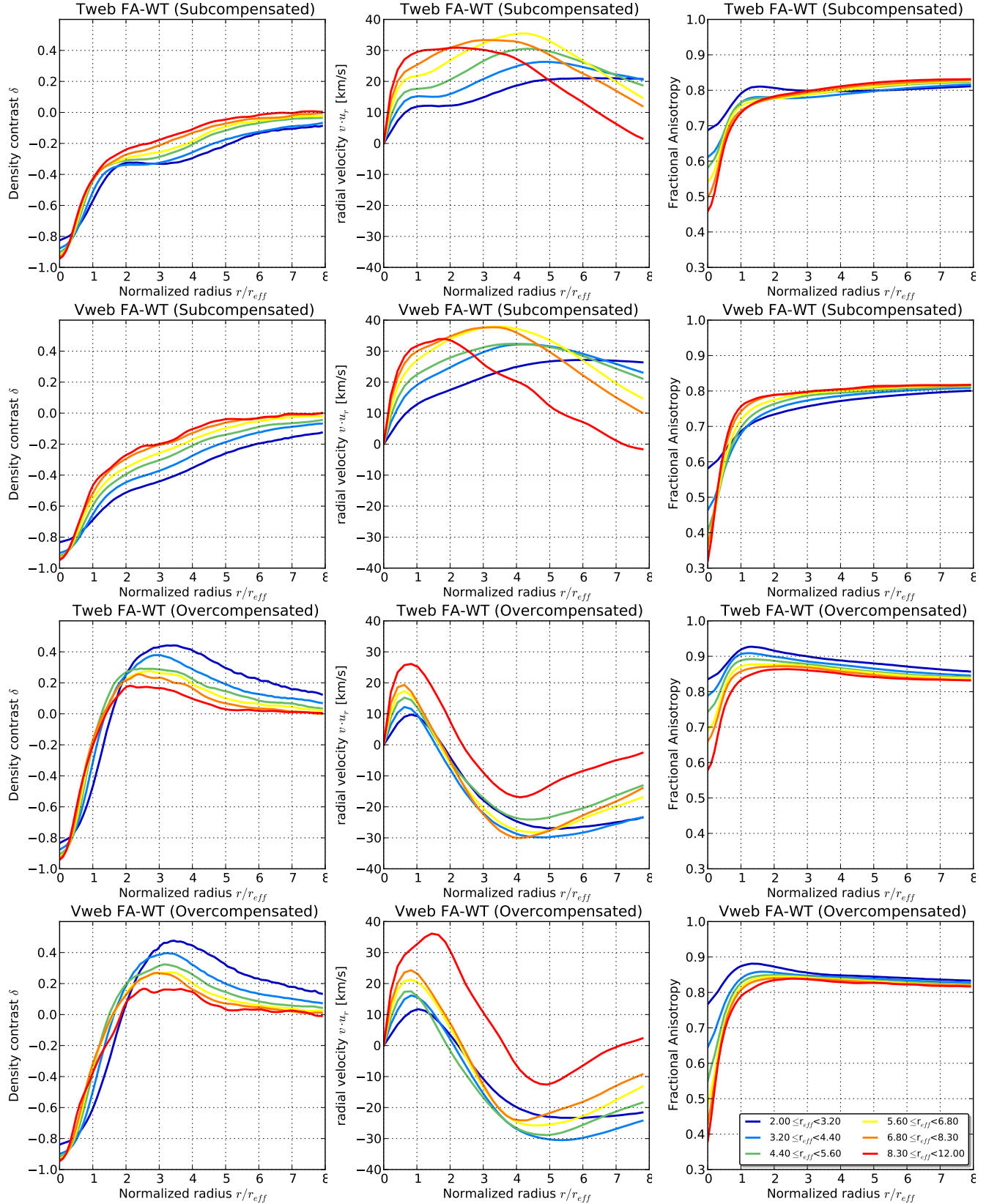
Figure 5. Density of voids for each finding scheme.